X-Ray Computed Tomography as a Method for Reproducing 3D Characteristics of Sulfides and Spinel Disseminated in Plagiodunites from the Yoko-Dovyren Intrusion

D. V. Korost[a], A. A. Ariskin[a, b], *, I. V. Pshenitsyn[a, b], and A. N. Khomyak[a]

[a]*Moscow State University, Moscow, 119234 Russia*
[b]*Vernadsky Institute of Geochemistry and Analytical Chemistry (GEOKhI),*
Russian Academy of Sciences, Moscow, 119991 Russia
*e-mail: ariskin@rambler.ru

Abstract—The paper describes a methodology of applying X-ray computed tomography (CT) in studying textural−morphological characteristics of sulfide-bearing ultramafic rocks from the Yoko-Dovyren layered massif in the northern Baikal area, Buryatia, Russia. The dunites are used to illustrate the applicability of a reliable technique for distinguishing between grains of sulfides and spinel. The technique enables obtaining statistical characteristics of the 3D distribution and size of the mineral phases. The method of 3D reconstructions is demonstrated to be applicable at very low concentrations of sulfides: no less than 0.1−0.2 vol %. Differences between 3D models are determined for sulfide segregations of different size, in some instances with features of their orientation suggesting the direction of percolation and accumulation of the sulfide liquids. These data are consistent with the morphology of the largest sulfide segregations, whose concave parts adjoin the surface of the cumulus olivine and simultaneously grow into grains of the poikilitic plagioclase. Detailed information of these features is useful to identify fingerprints of infiltration and concentration of protosulfide liquids in highly crystallized cumulate systems.

Keywords: X-ray computed tomography, disseminated sulfides, spinel, intrusion, 3D distribution, infiltration of sulfide liquids

DOI: 10.1134/S0869591119040040

INTRODUCTION

Complexes of mafic and ultramafic rocks are important sources of Ni, Cu, Pt, Pd, and some other transition and precious metals. The behavior of these elements in the course of the differentiation of mafic−ultramafic magmas is usually controlled by a sulfide phase, which is their dominant concentrator. Because of this, conditions at which sulfides are formed, distributed, and accumulated in lava flows and intrusive bodies are believed to be of a key importance for understanding the origin of magmatic Cu−Ni−PGE deposits and for developing exploration guides (Naldrett, 2004; Maier, 2005; Likhachev, 2006; Holwell and McDonald, 2010; McCuaig et al., 2010; Ripley and Li, 2013). Currently known examples include large layered plutons (such as Bushveld, Stillwater, or Monchapluton) and thinner bodies, which often occur as parts of volcano-plutonic complexes, such as intrusions in the Norilsk area in northern Siberia, the Duluth Complex in the United States, and Pechenga in the Murmansk Region in the Kola Peninsula, Russia (Cawthorn, 2005; Barnes and Lightfoot, 2005; Smolkin et al., 2004; Krivolutskaya, 2016). The geo-

logical−tectonic settings of the bodies, the structures and textures of rocks in the mineralized units, and the inner structures of the orebodies are different. The orebodies are conventionally classified into four major groups (Barnes et al., 2017): (1) stratiform units with sulfides, which are disseminated in the various cumulates of the layered inclusions, including PGE reefs; (2) globular and net-textured ores in relatively thin bodies, which are crystallized relics of the magma conduits; (3) sulfide accumulations in komatiite flows, which are also related to ultramafic magma feeders; and (4) mineralized zones in the peripheries of intrusive bodies, which are transitional from disseminated to globular ores (see, for example, Ariskin et al., 2018b; Karykowski et al., 2018). A separate type is the Sudbury deposit in Ontario, Canada, which was produced in a large impact structure (Naldrett, 2004).

Regardless of the fabrics of the mineralized rocks and the reserves of the sulfides, all of these types are genetically related to the phenomenon of silicate−sulfide liquid immiscibility, which emerges during various evolutionary episodes of the intrusive magmas and cumulates as their heterogeneous derivatives. The

onset of silicate–sulfide liquid immiscibility predetermines the sequence of the ore-forming processes, including the effective extraction, transfer, and accumulation of Cu, Ni, PGE, and other chalcophile elements in differentiation products of the magmas (Naldrett, 2004). The magmatic nature and composition of these initial sulfide liquids predestinate the later history of crystallization and subsolidus transformations of the protosulfide material, whose final mineralogical composition is dominated by pyrrhotite/troilite, pentlandite, and chalcopyrite ± cubanite of different generations (Spiridonov, 2010). Information on the sulfide-liquid prehistory of the ore-bearing systems can thus be understood by studying the complicated sulfide aggregates (including droplets, primary veinlets, network texture, and other shapes) and their bulk composition. The morphologies of the sulfide segregations reflect physical processes that were responsible for the transport and accumulation of the protosulfide liquids in the intergranular space of the partly crystallized cumulates (Ariskin et al., 2016; Barnes et al., 2017). The weighted mean chemical composition of the sulfides thereby reflects the evolution of the multicomponent Cu–Ni–Fe–PGE precursor in the course of the progressively developing liquid immiscibility (Campbell and Naldrett, 1979; Ariskin et al., 2018c) or during postcumulus crystallization and the subsequent separation of later Cu-rich Cu–Ni–Fe sulfide fractions (Mungall, 2002; Sinyakova and Kosyakov, 2012; Sinyakova et al., 2017).

Current models of sulfide–silicate liquid immiscibility are able to reasonably predict the ranges of thermodynamic parameters (T–fO_2–volatiles) responsible for the origin of sulfides in mafic–ultramafic systems (Li and Ripley, 2009; Fortin et al., 2015), including the composition of the starting Ni- and Fe-rich sulfide liquids (Ariskin et al., 2013). This fact has initiated the development of efficient algorithms for modeling conditions of melt saturation with sulfides and the evolution in the concentrations of PGE and chalcophile elements in magmatic melts and sulfide phases (Kiseeva and Wood, 2013, 2015; Ariskin et al., 2016, 2017, 2018a, 2018b). However, principally important aspects of ore-forming processes concern mechanisms responsible for the segregation, transfer, and accumulation of sulfide material in magmatic rocks. Impressive progress was achieved lately in understanding the nature of these transport phenomena, with regard for the interrelations between the physical parameters of the sulfide liquids and the rheological characteristics of the melt–crystal mixtures in which the very first sulfide globules and segregations are formed (Robertson et al., 2016; Barnes et al., 2017). An important role in pursuing this avenue of knowledge was played by experiments on the pore migration of sulfide melts in olivine cumulates, in combination with analysis of mechanisms of the microglobular and microsegregational deposition of condensed sulfides in a heterogeneous matrix (Mun-

gall and Su, 2005; Chang and Mungall, 2009). The results of these experiments have shown that the efficiency of material transfer and the initial accumulation of sulfides in magmatic rocks depends not only on the composition of the systems but also on the permeability of the cumulates when they are formed and during postcumulus processes, likely until the complete solidification of the rocks (Mungall, 2002). A fundamentally important conclusion is that, in spite of the fact that the wetting of silicate phases with sulfide liquid is low (which seems to preclude the downward migration of the globules larger than the intercumulus pores), the high density of sulfides as compared to that of the rock-forming minerals results in local hydrodynamic instability of the sulfide segregations (Robertson et al., 2016) and leads to their downward 3D transport through the pore space filled with intercumulus melt (Chang and Mungall, 2009).

Evidence for these processes is found not only in morphological features of the sulfide segregations but also in the structures of the cumulates and in the distribution of sulfide phases in the vertical sections of differentiated lava flows, layered intrusions, and related hypabyssal bodies (Keays et al., 2011; Holwell and Keays, 2014; Ariskin et al., 2016, 2018b). Techniques of modern X-ray computed tomography (referred to as CT below) make it possible to identify and quantitatively document these textural–structural characteristics (Baker et al., 2012; Pearce et al., 2017). The potentialities of such approaches have been demonstrated by studies of mineralized rocks from units with Pt mineralization in Bushveld and Stillwater (Godel et al., 2006), komatiites in western Australia (Barnes et al., 2008), and sulfide-enriched ultramafic rocks in the Mirabela Massif in eastern Brazil (Barnes et al., 2011).

Systematic progress in CT studies and their application to a broad spectrum of ore-bearing objects resulted in the development of a certain methodology for studies of mineralized rocks, with this methodology combining various X-ray techniques for the visualization of 3D structures and the capabilities of the 2D mapping of element concentrations in rock fragments with disseminated sulfides (Barnes et al., 2016, 2017). This publication presents our first results acquired by means of CT studies of sulfide-bearing ultramafic rocks from the bottom portion of the Yoko-Dovyren Massif in the northern Baikal area. The information was obtained by instrumental systems yielding data of different resolution and significance. Considering that systematic X-ray computed tomography studies of rocks were launched in Russia just lately, below we explain the fundamentals of this technique, with much attention paid to methodological issues related to difficulties in distinguishing between spinel and sulfides and interpretations of the 3D distribution of the sulfide phases.
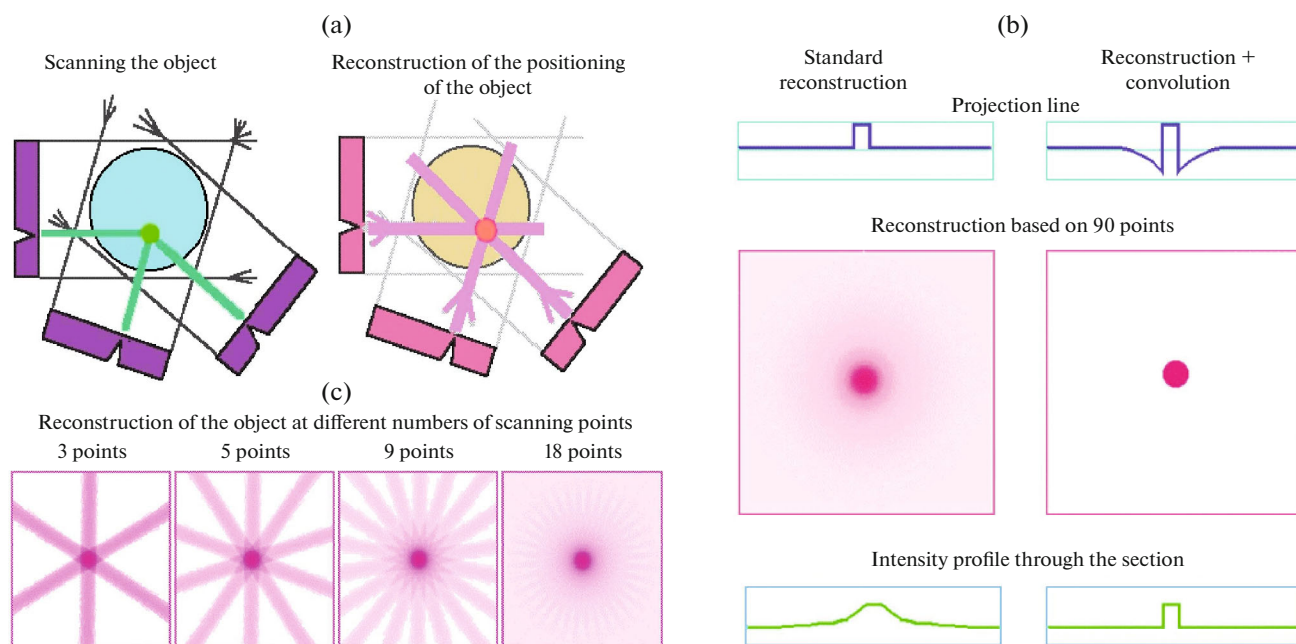
Fig. 1. Process flow diagram for X-ray scanning and reconstruction of data of the CT studies. (a) Principles used to reconstruct the positioning of the sample; (b) example illustrating the use of the convolution procedure; (c) influence of the number of the scan points on the reconstruction data.

METHODOLOGY AND EQUIPMENT FOR CT STUDIES

A principal task of computed tomography of rocks is noninvasive studying objects to acquire 3D models of their structure, determining textural relationships, and the morphology and distribution characteristics of the X-ray contrast phases. The advantages and limitations of these methods compared to the use of 2D representations of magmatic rocks in the form of thin sections and polished sections are discussed in (Baker et al., 2012), in which attention is attracted to the fact that the extrapolations of 2D information to a 3D "image" of the rock may lead to significant distortions relative to the real 3D textures and distribution because of the variations in the shape and size of the mineral grains and their aggregates. CT studies make it possible to minimize these uncertainties by using samples of different size (commonly, their size ranges from that comparable to conventionally used borehole core samples to small fragments and minicore ranging from 50 to 100 mm^3) and variations in the resolution from a few hundred to a few micrometers. These differences predetermine the specifics of X-ray macro- and microtomorgaphy, which are discussed below.

Fundamentals of the application of CT methods. The principal units of a computer tomography is a source of the X-ray radiation, an object to be studied, through which the emanated rays pass, and a detector, which records the level of radiation not absorbed by the object (Fig. 1). An individual 2D image, which corresponds to the intensity of X-ray radiation that passed through the studied sample, is referred to as a *shadow projection*. The fundamental principle is that numerous projections of the type are acquired from different angles, and hence, unlike classic X-ray radiography, this method makes it possible to record information not only on the projection of the sample but also on the 3D position of the object to be studied, the source, and the detector. Most state-of-the-art tomographs are third-generation equipment, in which the sample is positioned within the field of view of the detector (which is usually an X-ray camera), and the shadow projections are accumulated as a result of the stepwise axial rotation of the sample (Feldkamp, 1986), with an individual projection recorded at each rotation.

Brightness, which is conventionally visualized as gray gradations, reflects in the shadow projection the weakening of the X-ray radiation due to the scattering and absorption of the signal (X-ray absorption) that has passed through the sample. The attenuation of the signal depends on the density and composition of the material[1] of the studied object. This effect is described by the Beer–Lambert law, which specifies how a monochromatic beam attenuates when passing through an absorbing material (Rontgen, 1989)

$$I(x) = I_0 e^{(-\mu x)},$$

---

[1] The composition is conventionally characterized by parameter *Z*, which is the "weighted mean" atomic number of a given material.

where I_0 is the initial intensity of the X-ray radiation, x is the thickness of the layer of the material through which the radiation passes, and μ is the absorption coefficient of the material. It should thereby be borne in mind that absorption of X-ray radiation passing through a sample can be associated with the following four types of interaction: photoelectric absorption, Compton scattering, origin of electron−positron, and coherent Rayleigh scattering (Halmshaw, 1991). In the instance of geological materials, which are studied using 100- to 200-keV sources, the main process responsible for the attenuation of the radiation is photoelectric absorption. In practice, information on processes associated with the attenuation of the radiation is required to reasonably accurately process the data. Photoelectric absorption is known to be proportional to Z^{4-5}, whereas absorption at Compton scattering (which occurs when the radiation energy is 5−10 MeV) is proportional to Z. As a consequence of this difference, rays of lower energy are more sensitive to differences in the sample composition compared to radiation of higher energy. For example, quartz and potassic feldspar have similar densities (2.65 and 2.59 g/cm³, respectively), but the absorption μ of the two minerals is remarkably different at low radiation energies because potassic feldspar contains heavier potassium atoms. Scanning modes at different radiation energies are useful for enhancing the X-ray contrast of certain mineral phases in the shadow projections.

Principles of CT data reconstructions. Each shadow projection obtained by scanning the sample is exactly positioned, and this makes it possible to conduct data "reconstruction" by means of recalculating a series of the acquired X-ray patterns into a set of density X-ray sections that portray the inner structure of the object. In fact, this is a mathematical procedure for transforming the X-ray patterns into 2D density X-ray sections. The most commonly applied reconstruction algorithm is filtered back projection, when the original data massif is subjected to convolution. Thereby the radiation intensity on the original X-ray patterns is transferred onto a CT plane (in the form of the distribution of gray gradations in sections), whose resolution depends on the computer system, and each shadow projection is successively laid on the coordinate grid according to its position during scanning (Fig. 1).

Equipment. In the course of this research, we utilized CT systems selected with regard for the formulated petrological problems. Thereby we took into account that an unbiased evaluation of the quality and need to use a certain X-ray tomography should rely not so much on the technical characteristics of the instrument as, primarily, on the specifics of the sample to be studied under the parameters of a given experiment. Empirical experience suggests that principally important parameters of the scans usually cannot be reached simultaneously at their extrema. On the one hand, the highest resolution (a few micrometers) required long-lasting (up to 10−20 h) scans even for small rock fragments, and hence, this high resolution practically cannot be reached for large samples. On the other hand, it is better to study structural features of large samples using "faster" systems of relatively low resolution (hundreds of micrometers). Thereby highly contrasting X-ray absorption in mineral phases cannot be obtained at high radiation energies.

Sequence of data acquisition. During the *first step*, the largest (up to 7 × 7 × 20 cm) and potentially most important samples of sulfide-bearing rocks were scanned on an RKT-180 (manufactured at GEOLOGIKA, Novosibirsk, Russia) tomograph, which was designed to study full-sized borehole core material and makes possible fast enough scanning of cylindrical samples (up to four to six per day). The resolution of the data (depending on the chosen operation modes of the detector camera) is 100−200 μm. Visual analysis of the shadow projections reveals the general features of the inner structure of the samples and enables the researcher to select the most promising samples and/or their parts with different degrees of accumulation and spatial separation of sulfide phases. This allowed us to select the most informative samples for their further studies. At the *second step*, these samples were examined on a Phoenix v|tome|x m300 (GE, United States) scanner. The increase in the scanning time and successive reconstructions and the construction of 3D models allowed us to significantly improve the quality of the acquired information: the resolution for samples of different size was 40 to 70 μm, and the contrast of the data made it possible to reliably distinguish between most of the X-ray contrast components of the rocks. During the *third step*, some samples of this selection were used to cut off cylinders 10 mm in diameter, which were then scanned on a SkyScan-1172 (Bruker, Germany) scanner. This allowed us to acquire data stacks at a resolution of about 3 μm.

Scans for each samples involved 1000 (at step 1) to 4000 (step 3) plane sections, whose X-ray diffraction patterns were then recalculated into density sections using software of SkyScan (DataViewer, CTAn, CTVol, and CTVox). The density sections portrayed the inner structure of the sample. The significant differences of the densities of aluminochromite (4.5−4.8 g/cm³) and sulfides (~4.2 for chalcopyrite, 4.6−4.7 for pyrrhotite/troilite, and 4.6−5.0 g/cm³ for pentlandite) and those of rock-forming silicates (2.6−3.4 g/cm³) ensured realism of the acquired distributions of the densest phases ranging from a few dozen to a few centimeters and to a few micrometers (see below).

SAMPLES FOR THE CT STUDIES

This publication presents results obtained for a few samples of ultramafic rocks from the Yoko-Dovyren (referred to as Dovyren below) layered massif in the northern Baikal area. In spite of their lean sulfide min-
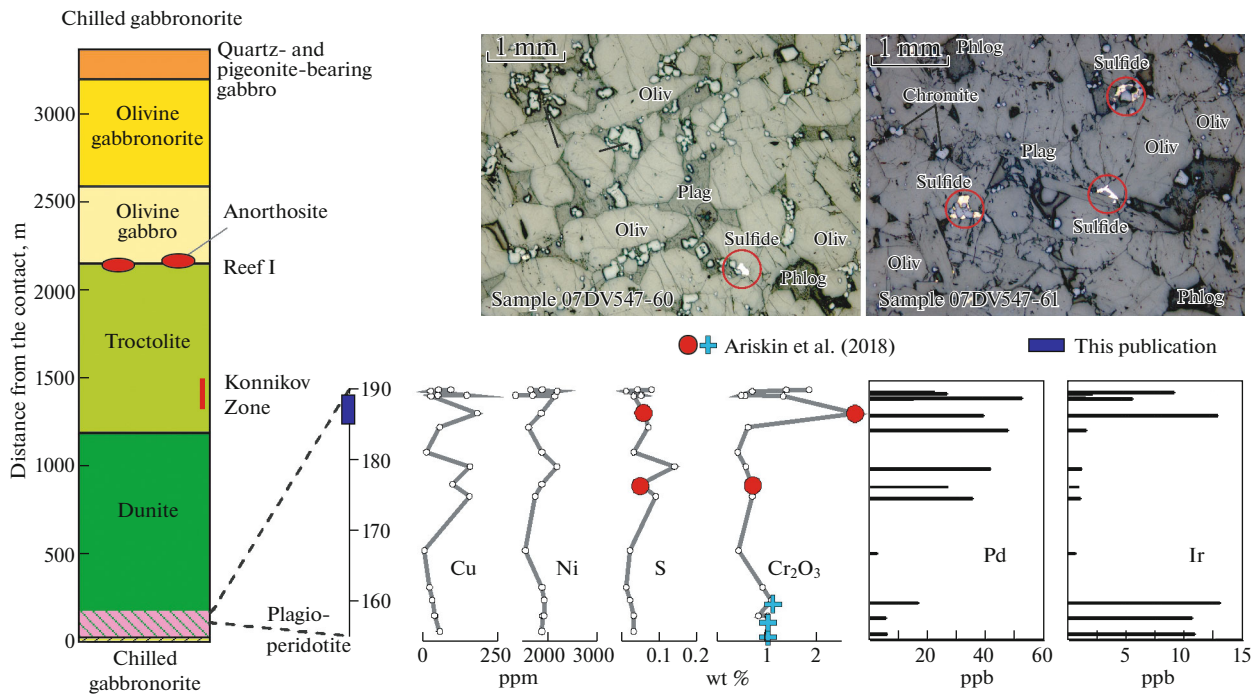
Fig. 2. Generalized vertical section of the central part of the Yoko-Dovyren Massif (Ariskin et al., 2016, 2018b), Cu, Ni, S, Cr₂O₃, and PGE distribution in the transition zone from plagiodunites to plagioclase-bearing dunites, and reflected-light micrographs of representative plagiodunite samples 07DV547-60 and -61. Pale blue crosses are type-I plagioperidotites or "plagiolherzolites", others symbols are as follows: the blue rectangle and red circles are type-II plagioperidotites or "plagiodunites" (Ariskin et al., 2018), in compliance with the locally conventionally assumed terminology for these rocks (Kislov, 1998).

eralization, these rocks are interesting as markers of early stages of silicate–sulfide liquid immiscibility during the crystallization of primitive Dovyren cumulates (Ariskin et al., 2018). Evidence of the process is provided by the Cu–Ni and PGE geochemistry of the rocks, indications that the cumulates are oversaturated with sulfur dissolved in the intercumulus melt relative to sulfides, and the character of the spatial distribution of chalcophile elements relative to other units in the bottom part of the layered series of the massif (Ariskin et al., 2018b, 2018c). The stratigraphic sequence of the Dovyren rocks is characterized below.

Inner structure and mineralization of the Dovyren Massif. The intrusion is located about 60 km north of the northeastern tip of Lake Baikal and is a roughly tabular body that extends from southwest to northeast for approximately 26 km (Konnikov, 1986; Kislov, 1998). The thickness of the massif varies from 1.3–2.2 km in its margins to 3.4 in the central portion, and its dip is nearly vertical. This is the largest body of the Dovyren intrusive complex, which was dated at 728 Ma and is a volcano-plutonic association referred to as the Synnyr–Dovyren Complex (Ariskin et al., 2009). This association comprises (along with the pluton itself) comagmatic sills and volcanics (Ariskin et al., 2013, 2015; Orsoev et al., 2018). The inner structure of Dovyren was best studied in its thickest central part, where more than 90% of the vertical section is made

up of a contrasting rock sequence, which can be correlated with a layered series (Fig. 2). It consists of units of plagioclase-bearing and adcumulus dunites in the bottom part (~970 m), troctolite of variable maficity in the middle part (~950 m), and overlying gabbroids, which vary from olivine gabbro to olivine and olivine-bearing gabbronorites (~1050 m). The lower part of the Layered Series grades into a plagioclase peridotite unit (in fact, olivine-rich gabbronorite, 150–200 m), which gives way to picritoid rocks (so-called picrodolerites) and chill gabbronorites near the lower contact. The top of the Layered Series is crowned by mostly olivine-free pigeonite-bearing gabbro and leucogabbronorites (~200 m), including fine-grained inner-contact facies of the rocks composing the roof of the body.

The Cu–Ni sulfide mineralization of Dovyren occurs as units with domains containing disseminated sulfides, which are unevenly distributed in the vertical section from the bottom to roof units (Kislov, 1998; Tolstykh et al., 2008; Ariskin et al., 2016, 2018b). Sulfide concentrations in some rocks reach 7–10 wt %. Ultramafic sills and gabbronorite dikes below the bottom of the intrusion and apophyses from the main body locally host rich disseminated and net-textured ores with up to 30% sulfides (Kislov, 1998).

Selection of representative samples. Our CT studies were carried out with the weakly and insignificantly

Table 1. Petrochemical characteristics of and concentrations of chalcophile elements in picrodolerite from the chill zone and in representative plagiodunite samples

No.	Sample	h, m	S, wt %	Cr_2O_3, wt %	Cu	Ni	Ir	Ru	Rh	Pd	Pt	Au
Picrodolerite from the chill zone at the lower contact of the intrusion												
1	DV30-1	0.4	0.05	0.17	70	555	1.07	3.13	0.75	8.44	7.12	1.52
Plagiodunites												
2	13DV547-59	186										
3	13DV547-60	187	0.06	2.78	180	1868	12.8	49.9	19.0	39.0	59.5	1.70
4	13DV547-61	188										
5	13DV547-62	189	0.03	1.31	25	2140	5.46	22.3	8.12	14.9	23.6	0.75
6	07DV124AB	190	0.05	0.47	48	1353	1.36	6.96	3.50	52.4	8.8	0.69

Sample numbers printed in semibold type are studied by CT methods, h is the distance from the lower contact of the massif (in m). PGE and Au concentrations are in ppb (analyses at the GEOLABS Laboratory, Ontario, Canada). Complete analyses of samples DV30-1, 13DV547-60, and -62, including the detection limits of elements are presented in (Ariskin et al., 2018). No data on the composition of samples 13DV547-59 and -61 are available, the composition of sample 07DV124AB is shown as a representative one for sampling the interval. The composition of sample DV30-1 can be viewed as an approximation of the composition of the initial Dovyren magma (Ariskin et al., 2018).

mineralized plagiodunite samples from a ~150-m unit in the bottom part of Dovyren (Ariskin et al., 2016). This unit was distinguished using elevated concentrations of Cu, Ni, Pd, Pt, Au, and other chalcophile elements in the rocks (Fig. 2). We ascribe these rocks to type 2 of relatively primitive plagioperidotites in the bottom part of the massif. They are transitional varieties between plagioclase lherzolites and plagioclase-bearing dunites with elevated contents of aluminochromite (Ariskin et al., 2018). The low-sulfide mineralization of the plagiodunites is rare disseminated sulfides between grains of the cumulus olivine, as part of the intercumulus association, which is strongly dominated by poikilitic plagioclase grains (Fig. 2). The sulfide phases are small (0.1−0.3 mm) polymineralic aggregates or larger (up to 1 mm) grains of pentlandite (up to 80−955) and pyrrhotite (which is a crystallization product of *Mss* with a broadly varying Fe/Ni ratio), with rare chalcopyrite. The rocks sometimes host larger aggregates of sulfides with phlogopite.

The sulfur concentration of the plagiodunites is comparable with those in rocks in the chill zone, although the latter contain much more intercumulus phases (Table 1). In other words, the plagiodunites are much richer in sulfur (normalized to the intercumulus mass). Moreover, comparison with SCSS (*Sulfur Content at Sulfide Saturation;* Campbell and Naldrett, 1979) predictive evaluations shows that these normalized concentrations in the Dovyren magma were notably higher than the possible limits of sulfide sulfur solubility in magmatic melt (Ariskin et al., 2018b). This means that the lean mineralization of the plagiodunites could not be formed in situ due to the local crystallization of sulfide phases from the intercumulus melt. We suggest that the sulfides were locally accumulated (in relatively small mass) in this unit as a consequence of the migration of immiscible sulfide liquid from higher levels through the pore space of the lower solidifying cumulates. This is consistent with positive correlations between the concentrations of PPGE, S, and Te in rocks in the bottom part of Dovyren, including picrodolerites from the contact and other weakly mineralized rocks in the bottom of the massif (Ariskin et al., 2018c). The plagiodunites with disseminated sulfide mineralization are thus a suitable subject for tomography studies aimed at searches for evidence of the percolation and accumulation of small portions of primitive sulfide melts.

Another important feature of these rocks is their elevated (as compared to other sulfide-bearing ultramafic rocks) Ir, Ru, and Rh concentrations, which are correlated with the highest (again, as compared to other sulfide-bearing rocks) concentrations of Cr (see Fig. 2 for the Ir and Cr_2O_3 distributions). Such correlations are related to the enrichment of the rocks in spinel, which is a phase concentrating IPGE and thus controlling the behavior of these elements before the onset and during silicate−sulfide liquid immiscibility (Ariskin et al., 2018). This feature calls for using the same samples to solve the problem of the 3D distribution of the spinel and strongly subordinate amounts of sulfides, which is a challenging task for CT studies.

The selection of samples for the solution of the formulated problems involved two steps. First, at a preparatory step, Dovyren ultramafic rocks were scanned on a RKT-180 low-resolution tomograph. These results were analyzed in search for microfracturing and the presence (or absence) of sulfide phases. The data thus acquired provided a basis for the final selection of four rocks from a 3-m interval in the bottom part of the plagiodunite unit (Table 1). For the microtomographic studies at a resolution of 40−70 μm, we have prepared five cube-shaped (~2 cm in edge) samples (Fig. 3), including samples 13DV547-59, -60, -61a, -61b, and -62 (Fig. 3). The further more detailed study at a

resolution of ~3 μm was carried out with cylinders 10 mm in diameter cut off these samples.

RESULTS

For each of the five selected samples, primary stacks were acquired, which consisted of two to three thousand X-ray density sections and were used to distinguish X-ray contrast components. These data were then utilized in stereological reconstructions of 3D models. Simultaneously we have statistically processed the distribution patterns of these components, including estimations of the volume contents, size distributions, connectivity, and morphological characteristics.

Studies at a resolution of 40−70 μm. Based on the CT data, three X-ray contrast phase associations[2] were distinguished: olivine (close to 80 vol %, likely with an admixture of pyroxene rims), dominantly plagioclase (occasionally with phlogopite), and Cr-spinel with vanishingly low amounts of sulfide, see Fig. 4 for an demonstrational different-density section of sample 13DV547-59. In spite of the relatively low contrast, successive processing of such stacks with the CTAn program code of the SkyScan software enables the researcher to acquire stereological models of samples that demonstrate the 3D distribution of the distinguished X-ray contrast phases, provisionally referred to as phase 1 (olivine), phase 2 (plagioclase), and phase 3 (spinel). Figures 5a−5c display the 3D distribution of plagioclase and spinel and the result of their combination in a single projection for sample 13DV547-59. In analyzing such stereograms, one shall be aware that, when 3D models are projected on a plane, a seemingly almost complete filling of the volume is reached at concentrations of the phase higher than 5−10%. This is illustrated by the plagioclase distribution in Fig. 5a, because the content of this mineral in the plagiodunites varies (according to CIPW calculations) from 13 to 15 vol % (Ariskin et al., 2018). This explains the absence of an analogous projection for olivine, which would have look as a cubic object of a single background color. Also, at a given resolution, phase 3 includes intercumulus spinel alone and no minor inclusions of this mineral in olivine, which are mostly smaller than 20−30 μm. For the same reason, groups of relatively small spinel inclusions in the poikilitic plagioclase (see photos of thin sections in Fig. 2) are usually merged in the X-ray images.

The CTAn program code in the SkyScan software makes it possible to calculate the mean volumetric contents of X-ray contrast phases and parameters of
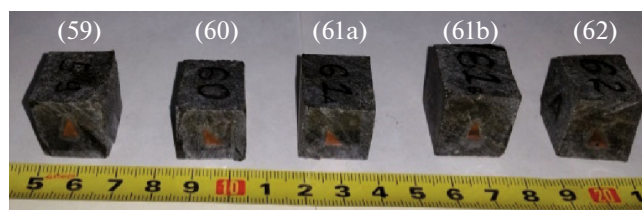
[2] At the initial stage of these studies, the term *phase* was used to denote mixture of components (which sometimes consisted of different mineral species) that have similar X-ray absorption characteristics at these scanning parameters, for example, the associations olivine ± pyroxene or spinel ± sulfide. The possibility of distinguishing between spinel and sulfide as individual mineral phases was provided by scans at higher resolution.

Fig. 3. Photos of the cube-shaped plagiodunite samples (13DV547-59, -60, -61a, -61b, and -62) manufactured for our detailed CT studies (Table 1).

their *connectivity* in the samples (Table 2)[3]. An important outcome of this numerical analysis is the conclusion that almost all of the poikilitic (in 2D sections) plagioclase is seen to form a continuous (in 3D representation) network that fills the space between the olivine grains. This follows from the high values of plagioclase connectivity: 90−95% (Table 2). Hence, all of the plagioclase can be viewed as an in-situ crystallization product in the intercumulus, and the volume filled with this mineral can be regarded as a sort of cast of the pore space of the olivine cumulates, which was filled with magmatic melt. At the same time, phase 3 (spinel + rare sulfides) occurs as numerous (on average, a few thousand) separate objects (Fig. 5b).

We have also statistically analyzed the shapes and sizes of the elements of the spinel. The shapes of the individual objects were estimated based on their relative *sphericity* (which is the S_1/S_2 ratio, where S_2 is the surface area of a given particle, and S_1 is the surface area of a sphere of the same volume). As it turned out, most of these objects are characterized by sphericity from 0.85 to 0.95 (Fig. 6). These estimates reflect the nearly spherical shapes of the 3D accumulations (clusters) of spinel grains in the intercumulus (left-hand photo of a thin section in Fig. 2).

To statistically compare the sizes of individual spinel elements of somewhat different shape, we applied another parameter acquired in CT studies: the so-called *effective diameter*. This parameter is interpreted as the diameter of a sphere whose volume is equal to that of a given object (Fig. 6a). It turned out that most objects interpreted as spinel have linear sizes of 100−400 μm (Fig. 7). This large average size of the distinguished elements of the mineral pertains not to individual grains but to their compact aggregates discernible at the resolution of the scans (see above).

Studies at a resolution of approximately 3 μm. To conduct more detailed scans, small cores, 10 mm in diameter, were sawn off the cubic samples and were then studied at the maximum resolution and lower central energy of the source. The CT data on these scans allowed us to reliably distinguish as many as four (but not only three) X-ray contrast phases, which

[3] *Connectivity* is understood herein as a fraction of the largest coherent object in the overall volume of a given phase.
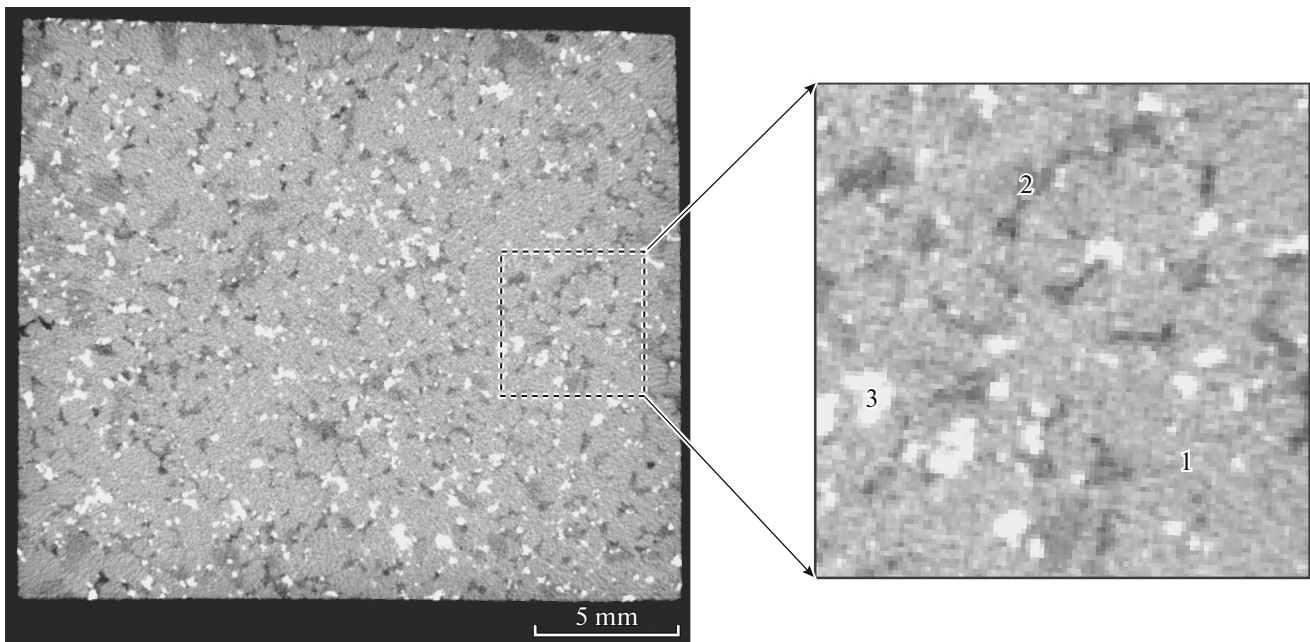
Fig. 4. Example of an individual X-ray density section of cubic sample 13DV547-59, resolution 40−70 µm. In the enlarged fragment: pale gray phase 1 (olivine), dark gray phase 2 (plagioclase), and white phase 3 (spinel).
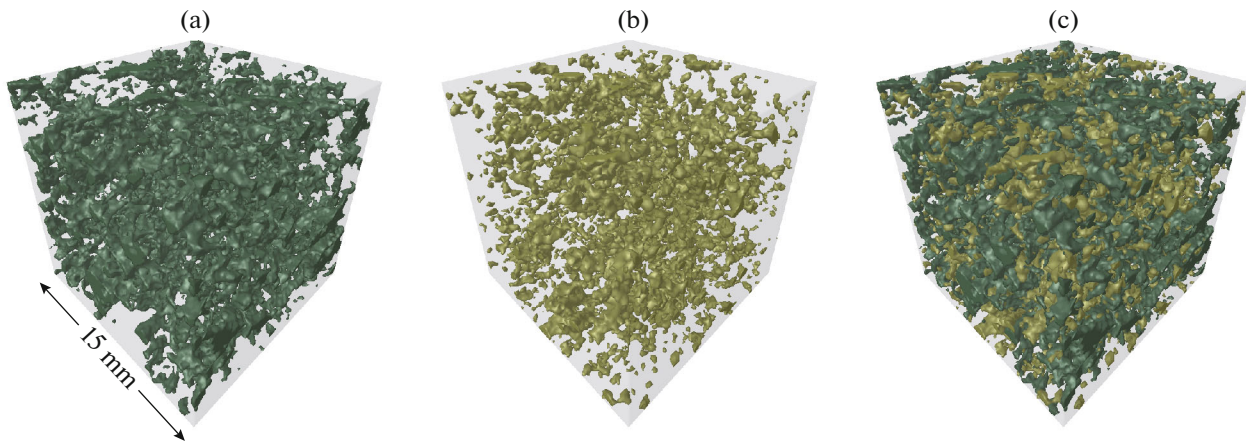

Fig. 5. Examples of 3D models for X-ray contrast rock-forming components of plagiodunite, sample 13DV547-59, resolution 40−70 µm. (a) Green phase 2 (plagioclase); (b) phase 3 (spinel); (c) combination of the plagioclase and spinel 3D distributions.

manifest themselves in the plane sections of sample 13DV547-62 and correspond to olivine (phase 1), plagioclase (phase 2), real spinel (phase 3), and sulfide (phase 4) (Fig. 8). This example shows that this set of experiments is characterized by a slightly lesser X-ray contrast between the olivine and plagioclase and by the possibility of reliable identification of two high-density phases: Al−Cr spinel (Ariskin et al., 2018) and sulfide. Thus, the improvement of the result on X-ray absorption is explained by the following two interrelated phenomena: the improvement of the spatial resolution and a decrease in the source energy, which leads to the dominance of photoelectric scattering.

Figures 9a−9d show the distributions of plagioclase, spinel, and sulfide and their combination in a single projection in a cube with a 2-mm edge, which was "numerically cut off" the cylinder. Note the band-shaped character of the sulfide segregations (Fig. 9c), which can be interpreted as a trace of the local filtration of sulfide liquid through the pore space of the cumulates (Ariskin et al., 2016). It is interesting that the termination of this continuous cluster is marked by the largest sulfide segregation. The absence of data on the spatial orientation of the sample does not allow us to determine whether these textural relationships

Table 2. Concentrations of X-ray contrast components in the cubic plagiodunite samples at CT scans at a resolution of 40−70 μm

Sample	Olivine ± rare pyroxene	Plagioclase + subordinate phlogopite amounts		Spinel + rare sulfides
	vol %	vol %	connectivity, %	vol %
13DV547-59	79.0	13.8	90	7.2
13DV547-60	81.8	15.5	92	2.7
13DV547-61a	83.2	13.3	91	3.5
13DV547-61b	81.8	15.8	95	2.4
13DV547-62	81.7	15.6	95	2.7

reflect the origin of this segregation or its break-up in the gravity field (Robertson et al., 2016).

Table 3 reports the volumetric contents of the four dominant mineral phases and the connectivity of the plagioclase in the 10-mm cylindrical samples. Similar to what was determined for the cubic samples, a high connectivity (94−97%) of plagioclase was determined for these samples too, but the estimated contents of the phases in the samples are somewhat different: within 1.5−5 vol % for olivine, 1.5−3% for plagioclase, and 0.1−2.6% for spinel. These variations may be explained by the heterogeneity of the original cubic samples and by differences due to the different resolution of the scans and the sizes of the objects. The estimated volumetric contents of sulfides in the plagiodunites with lean sulfide mineralization are in reasonably good agreement with data on the sulfur concentrations in the rocks: for example, the rock of sample 13DV547-60 contains 0.06 wt % sulfur (Table 1),
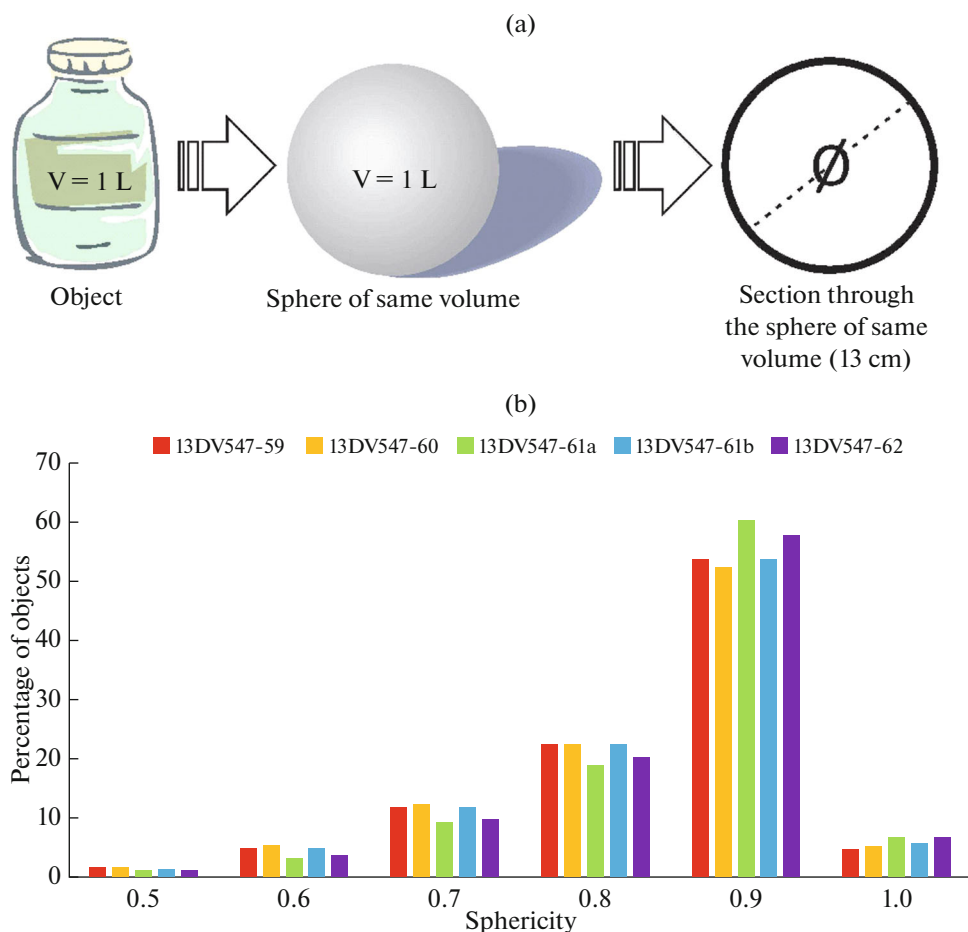

Fig. 6. (a) Graphical example of calculating the equivalent diameter of an object of geometrically irregular shape and (b) histograms showing the distribution of clusters and crystals of phase 3 (spinel) according to their sphericity in the cubic samples.
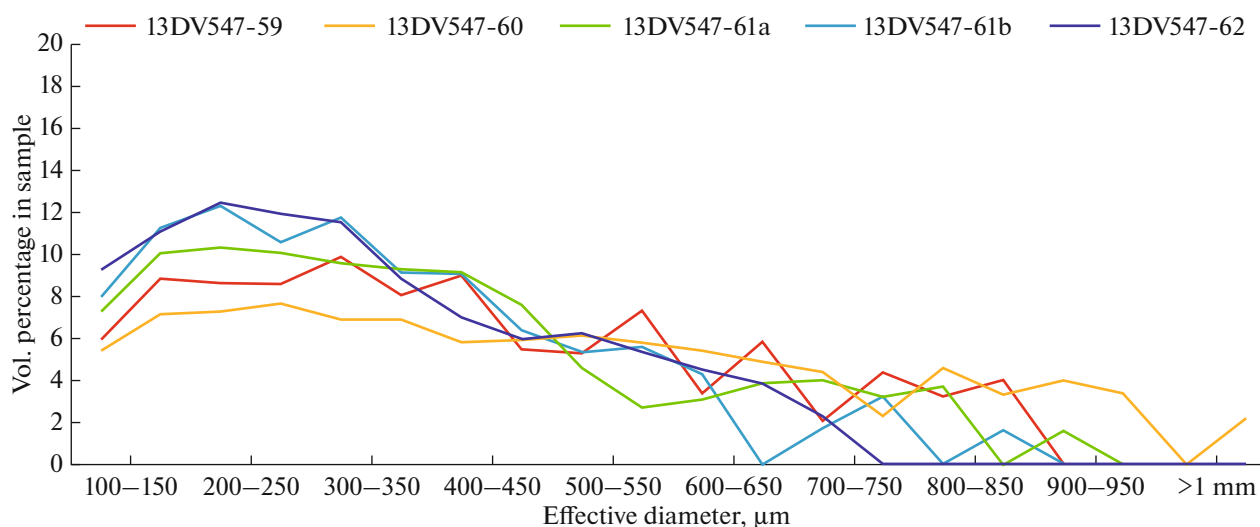
Fig. 7. Size distribution of individual "spinel" particles (crystals + grain clusters) in the cubic samples.
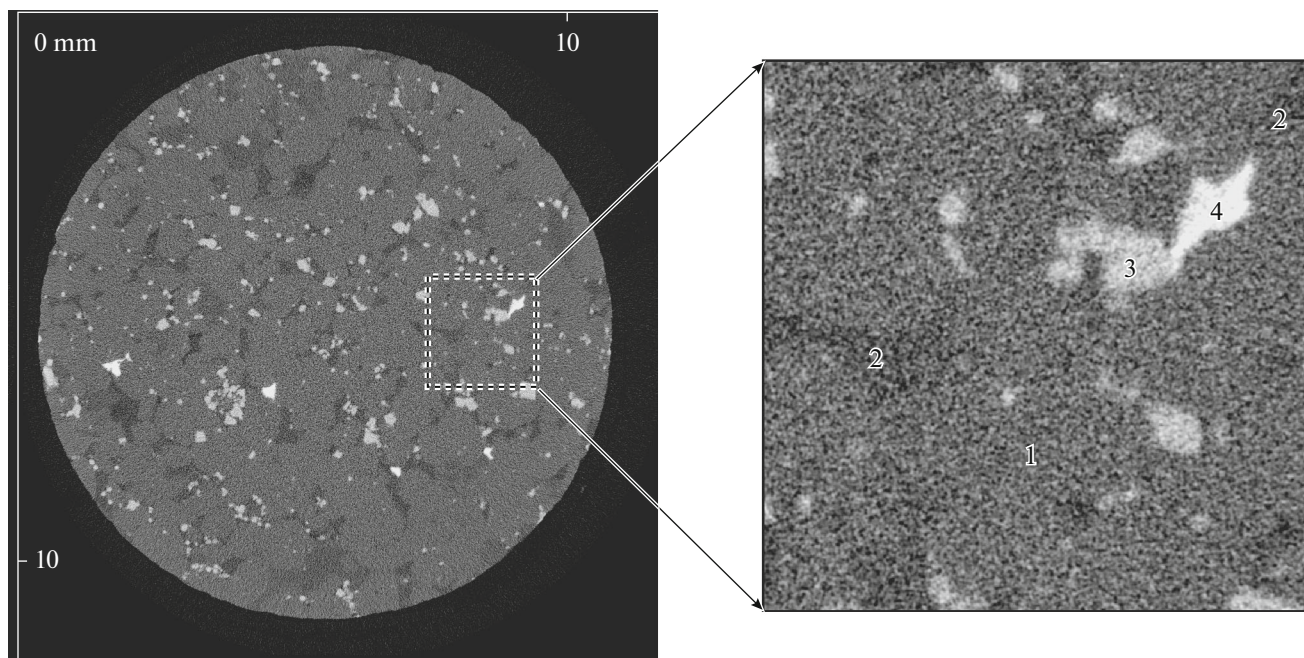

Fig. 8. Example of an X-ray density section for plagiodunite cylindrical sample 13DV547-62 (diameter 10 mm), resolution about 3 μm. In the enlarged fragment: phase 1 (olivine), phase 2 (plagioclase), phase 3 (spinel), and phase 4 (sulfide).

the average sulfur concentration in sulfide is 35 wt %, i.e., the rock contains at least 0.06/0.35 = 0.17 wt % sulfide. By recalculating wt % in vol % (with regard for the high density of sulfide), we arrived at a value slightly higher than 0.1 vol %, which is consistent with the estimate of 0.07 vol % based on CT data (Table 3).

In analyzing the sphericity and size distribution of spinel grains and clusters, elements making up this phase were combined with those of the sulfide phase, considering its negligibly low content. This allowed us

to directly compare data on the cylindrical and cubic samples in which we failed to distinguish between sulfides and spinel. Estimates of the sphericity of these elements acquired by scanning different samples at different resolution are generally close but not exactly identical (compare the histograms in Figs. 6 and 10). The numbers of clusters with high sphericity coefficients of 0.8–1 for cubic samples scanned at a relatively low resolution are greater than 90% on average (Fig. 6), whereas high-resolution scans of the cylindri-
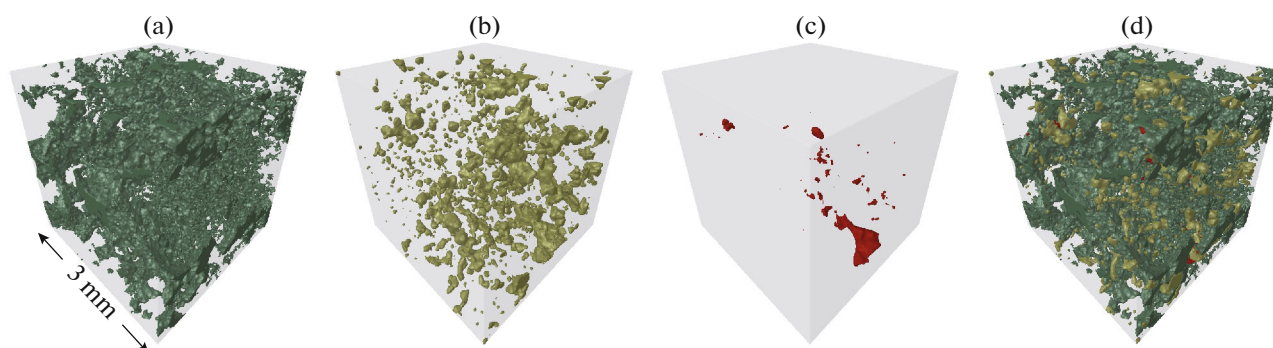
Fig. 9. Examples of 3D models for X-ray contrast rock-forming components of plagiodunite, sample 13DV547-62, resolution about 3 μm. (a) Phase 2 (plagioclase); (b) phase 3 (spinel); (c) phase 4 (sulfide); (d) combined distributions of plagioclase, spinel, and sulfide.
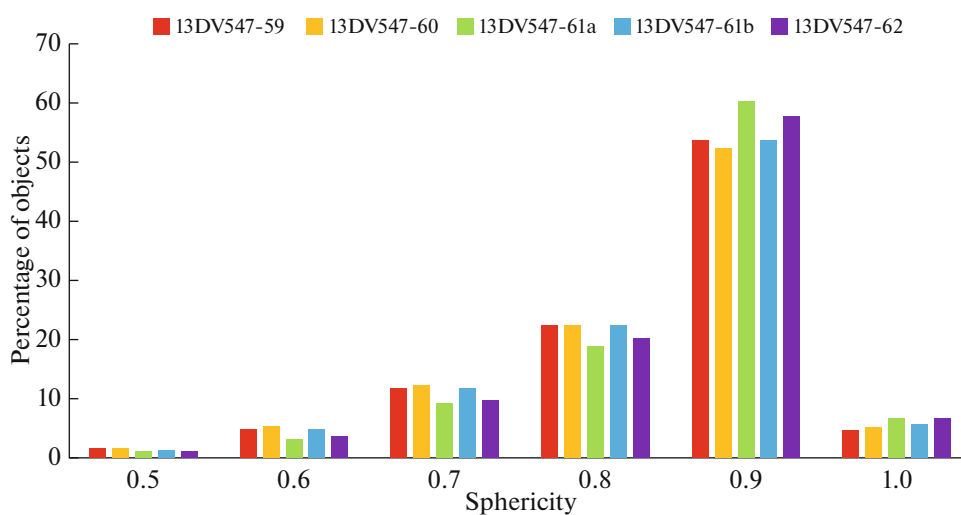

Fig. 10. Histograms of the distribution of individual elements of a composite phase (spinel + sulfide) according to its sphericity in the cylindrical samples.

cal samples yielded estimates close to 80% (Fig. 10). This suggests that high-resolution CT data make it possible to subdivide some of the clusterized elements but do not yield as much details as optical microscopy can provide (Fig. 2).

The distribution of the estimated "average" (equivalent) size of spinel elements are distinguished much more contrastingly, particularly within the range of 100–400 μm and for maximum sizes larger than 700 μm (compare Figs. 7 and 11). For the cubic samples, the

Table 3. Concentrations of X-ray contrast components in the cylindrical plagiodunite samples at CT scans at a resolution of about 3 μm

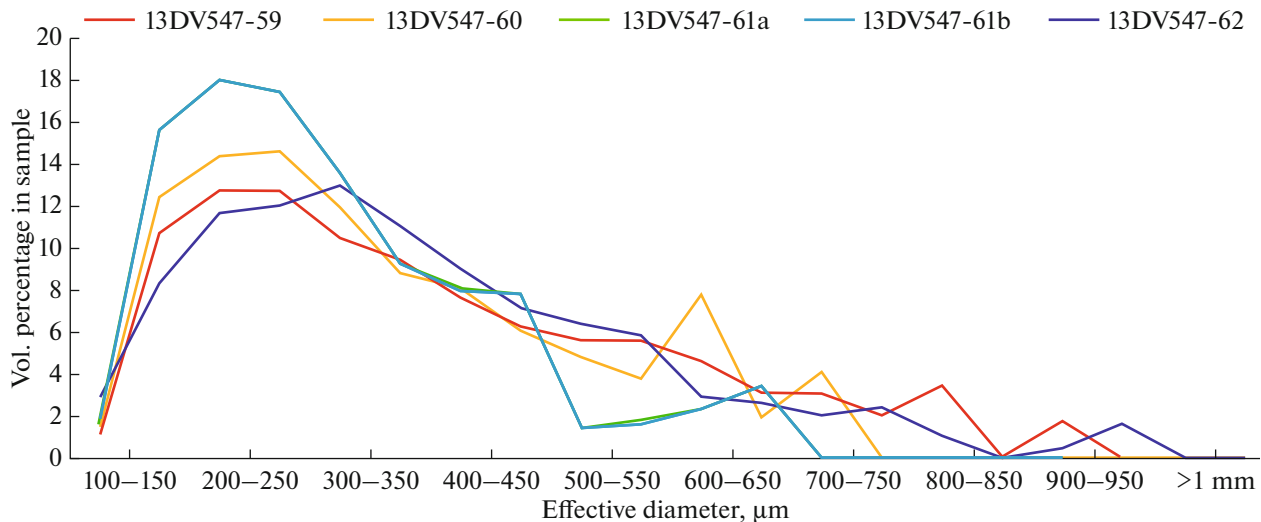| Sample	Olivine	Plagioclase		Spinel	Sulfide
	vol %	vol %	connectivity, %	vol %	vol %
13DV547–59	84.48	10.80	94	4.60	0.12
13DV547–60	80.73	14.10	97	5.10	0.07
13DV547–61a	86.15	10.00	95	3.80	0.05
13DV547–61b	84.95	11.90	96	3.10	0.05
13DV547–62	80.35	17.00	97	2.60	0.05

Fig. 11. Distribution of composite phase (spinel + sulfide) according to its size in the cylindrical samples.

size distribution curves for the former range look monotonous and display a tendency toward a systematic decrease from approximately 12% for elements 150−200 μm in size to 8% for the size range of 350−400 μm (Fig. 7). For the cylindrical samples and scans at higher resolution, the curves show clearly seen extrema corresponding to 16−18% elements 150−300 μm in size and a drastic decrease for clusters larger than 700 μm (Fig. 11). This obviously reflects the fact that a higher resolution makes it possible to differentiate artificially combined clusters into fragments of smaller size, including those corresponding to real larger spinel grains (see photos of thin sections in Fig. 2).

Distribution and morphology of sulfide grains in the plagiodunites. The fact that our samples contain very low concentrations of sulfide phases (a few hundredths of a percent) (Table 3) makes it possible to visualize the morphological diversity of the sulfide elements, the largest of which (up to 1 mm across) were detected in the cylindrical samples 13DV547-59 and -61a (Fig. 12). The 3D reconstructions presented herein demonstrate differences in the 3D distribution of sulfides: samples 13DV547-60, -61b, and -62 are characterized by a more even size distribution of the grains and volume filling, whereas samples 13DV547-59 and -61a not only demonstrate the presence of the largest segregations but also indications of their preferable orientation, similar to that in Fig. 9c. Thereby the largest sulfide segregations were found at the lowermost stratigraphic level, in sample 13DV547-59 (Table 1). The morphology of these large grains is diverse: they always occur as irregularly shaped branching aggregates, whose concave fragments suggest that the grains of the rock-forming olivine and plagioclase were "encapsulated" (Fig. 13).

This shape leaves little doubt that these segregations were produced by the crystallization of the orig-

inal sulfide liquids, which were locally concentrated in the intergranular space of the cumulus olivine and plagioclase and crystallized in situ, likely simultaneously with the progressively developing sulfide−silicate liquid immiscibility. This is also consistent with the spatial association of the sulfides with other intercumulus phases, first of all, plagioclase. For example, Fig. 14 displays stereological relationships between large sulfide particles and plagioclase in a number of cubic volumes "cut off" programmatically from cylindrical sample 13DV547-59 (Fig. 12). These results demonstrate that sulfide segregations in the rock form, together with plagioclase, a continuous branching network in the intergranular space between the cumulus olivine (Fig. 14). This is consistent with the hypothesis that such relationships between intercumulus phases provide a record of the origin, infiltration, and migration of sulfide melts through the pore space of crystallizing cumulates (Barnes et al., 2017).

CONCLUSIONS

(1) Practical aspects of the application of X-ray computed macro- and microtomography are discussed in the context of studying the textural features and morphology of sulfide and spinel grains in weakly mineralized ultramafic rocks, as exemplified by plagiodunites of the Yoko-Dovyren layered massif. It is demonstrated that these phases in the rocks can be reliably distinguished by varying the resolution and energy of the source, and statistically justified textural−petrographic characteristics of these phases can thus be presented. This approach is determined to be able to yield realistic estimates of the contents of sulfide phases, up to their very low concentrations of about 0.1−0.2 wt %.
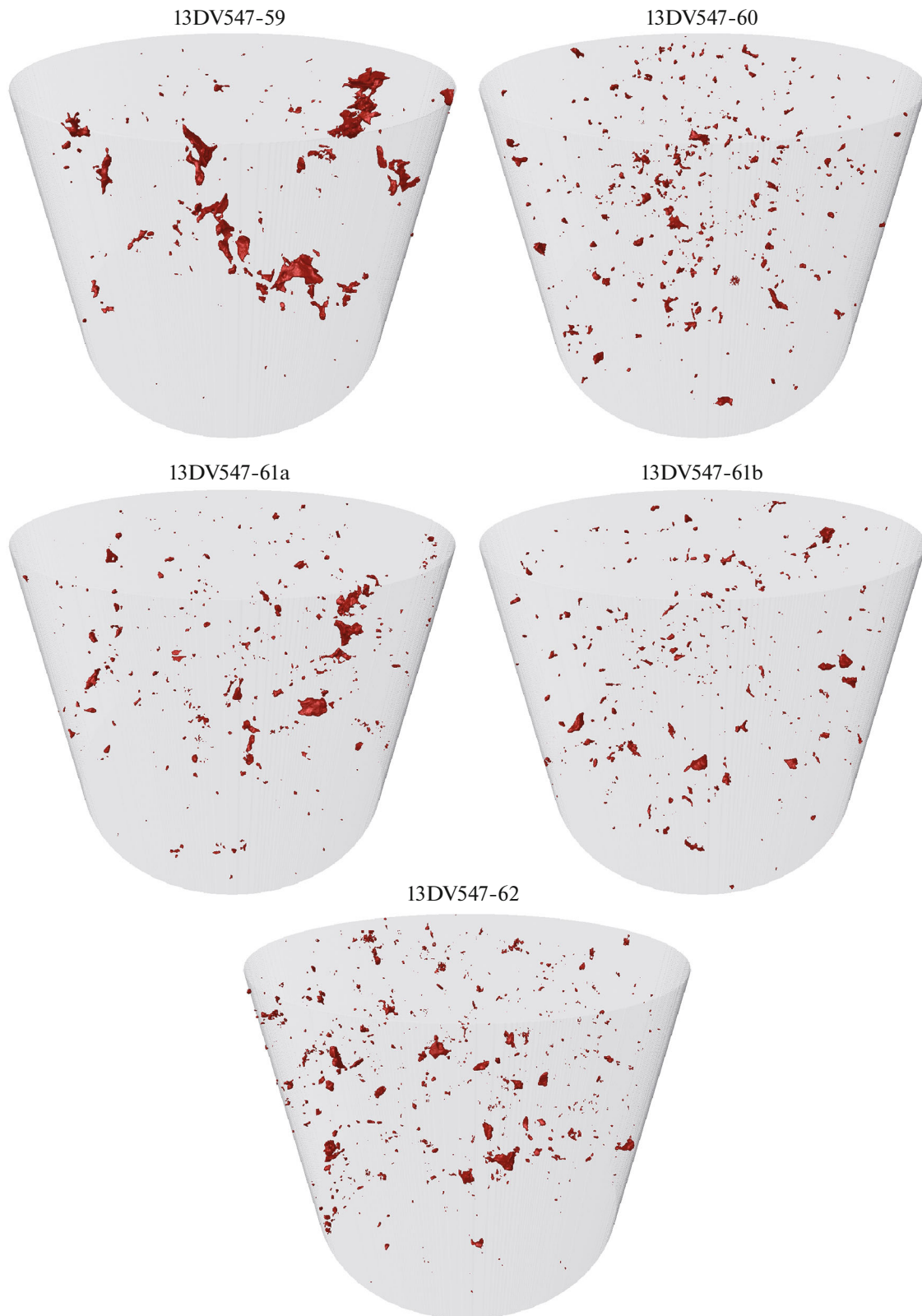
13DV547-59   13DV547-60

13DV547-61a   13DV547-61b

13DV547-62

Fig. 12. 3D distribution models of sulfide particles in the cylindrical samples. The cylinders were 10 mm in diameter. Sample numbers correspond to series 13DV547-nn (Table 1). Animations of the 3D distribution of sulfides in samples 13DV547-59 and 13DV547-62 are presented as ESM-1.pdf and ESM-2.pdf at http://link.springer.com.

←0.5 mm→

Fig. 13. 3D models of the largest particles of the sulfide phase in the plagiodunite samples.
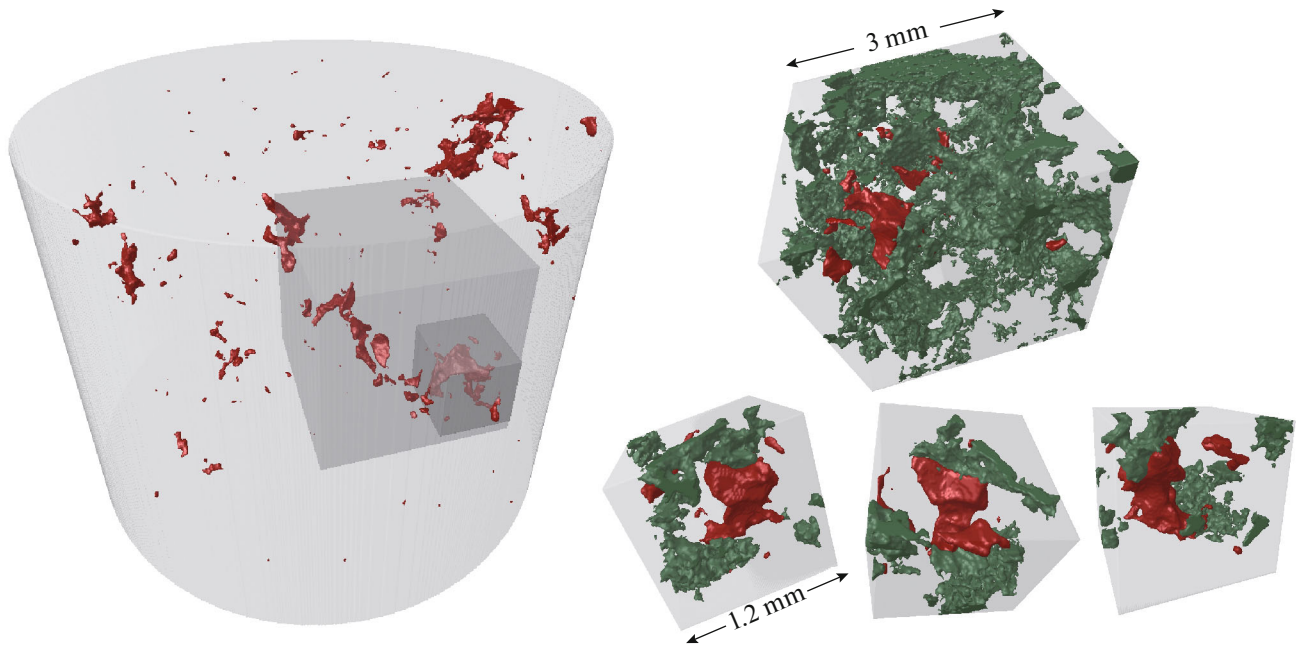

3 mm

1.2 mm

Fig. 14. 3D models of relationships between the intercumulus plagioclase (green) and large sulfide segregations (red) in sample l3DV547-59.

(2) Visual analysis of stereological models of the distribution of the sulfide phases indicates that the sulfide segregations of different size show a certain preferable orientation (Fig. 9c), and the largest of these segregations are spatially constrained to contacts with the surface of cumulus olivine crystals (Fig. 13) and ingrow into grains of the poikilitic (intercumulus) plagioclase (Fig. 14).

(3) The shape and distribution of the largest sulfide segregations provides a record of the prehistory of the sulfide liquids, which were concentrated in the residual pore space of the crystallizing cumulates and sometimes formed chains, interpreted as trails of pathways of higher permeability.

(4) More detailed information on the morphology of, and understanding physical reasons for the origin of these textures are useful for searching for fingerprints of infiltration and concentration of primary magmatic sulfide liquids in highly crystallized cumulate systems.

(5) A promising avenue of modern petrology is correlation between the results of CT studies of this type with information on the geochemical specifics of the behavior of chalcophile elements (PGE among others) during differentiation of mafic−ultramafic magmas in large magma chambers (Ariskin et al., 2017, 2018c).

REFERENCES

Ariskin, A.A., Bychkov, K.A., and Nikolaev, G.S., Modeling of trace-element composition of sulfide liquid in a crystallizing basalt magma: development of the *R*-factor concept, *Geochem. Int.,* 2017, vol. 55, no. 5, pp. 411−434.

Ariskin, A.A., Danyushevsky, L.V., Konnikov, E.G., et al., The Dovyren intrusive complex (northern Baikal region, Russia): isotope-geochemical markers of contamination of parental magmas and extreme enrichment of source, *Russ. Geol. Geophys.,* 2015, vol. 56, no. 3, pp. 528−556.

Ariskin, A.A., Konnikov, E.G., Danyushevsky, L.V., et al., The Dovyren Intrusive Complex: Problems of Petrology and Ni Sulfide Mineralization, *Geochem. Int.,* 2009, vol. 47, no. 5, pp. 425−453.

Ariskin, A.A., Konnikov, E.G., Danyushevsky, L.V., et al., Geochronology of the Dovyren intrusive complex, northwestern Baikal Area, Russia, in the Neoproterozoic, *Geochem. Int.,* 2013, vol. 51, no. 11, pp. 859−875.

Ariskin, A.A., Nikolaev, G.S., Danyushevsky, L.V., et al., Geochemical evidence for the fractionation of iridium group elements at the early stages of crystallization of the Dovyren magmas (northern Baikal area, Russia), *Russ. Geol. Geophys.,* 2018, vol. 59, no. 5, pp. 411−434.

Ariskin, A.A., Danyushevsky, L.V., Bychkov, K.A., et al., Modeling solubility of Fe−Ni sulfides in basaltic magmas: the effect of Ni in the melt, *Econ. Geol.,* 2013, vol. 108, no. 8, pp. 1983−2003.

Ariskin, A.A., Kislov, E.V., Danyushevsky, L.V., et al., Cu−Ni−PGE fertility of the Yoko−Dovyren layered massif (northern Transbaikalia, Russia): thermodynamic modeling of sulfide compositions in low mineralized dunites based on quantitative sulfide mineralogy, *Mineral. Deposita,* 2016, vol. 51, pp. 993−1011.

Ariskin, A.A., Bychkov, K.A., Nikolaev, G.S., and Barmina, G.S., The Comagmat-5: modeling the effect of Fe−Ni sulfide immiscibility in crystallizing magmas and cumulates, *J. Petrol.,* 2018a, vol. 59, no. 2, pp. 283−298.

Ariskin, A., Danyushevsky, L., Nikolaev, G., et al., The Dovyren intrusive complex (southern Siberia, Russia): insights into dynamics of an open magma chamber with implications for parental magma origin, composition, and Cu−Ni−PGE fertility, *Lithos,* 2018b, vol. 302−303, pp. 242−262.

Ariskin, A.A., Nikolaev, G.S., Danyushevsky, L.V., et al., Genetic interpretation of the distribution of PGE and chalcogens in sulfide-mineralized rocks from the Yoko-Dovyren layered intrusion, *Geochem. Int.,* 2018c, vol. 56, no. 13, pp. 1322−1340.

Baker, D.R., Mancini, L., Polacci, M., et al., An introduction to the application of X-ray microtomography to the three-dimensional study of igneous rocks, *Lithos,* 2012, vol. 148, pp. 262−276.

Barnes, S.-J. and Lightfoot, P.C., Formation of magmatic nickel−sulfide ore deposits and processses affecting their copper and platinum−group element contents, Hedenquist, J.W., Thompson, J.F.H., Goldfarb, R.J., and Richards, J.P., Eds., *Econ. Geol.,* 2005, vol. 100, pp. 179−213.

Barnes, S.J., Fiorentini, M.L., Austin, P., et al., Three-dimensional morphology of magmatic sulfides sheds light on ore formation and sulfide melt migration, *Geology,* 2008, vol. 36, pp. 655−658.

Barnes, S.J., Osborne, G., Cook, D., et al., The Santa Rita nickel sulfide deposit in the Fazenda Mirabela Intrusion, Bahia, Brazil: geology, sulfide geochemistry and genesis, *Econ. Geol.,* 2011, vol. 106, pp. 1083−1110.

Barnes, S.J., Cruden, A.R., Arndt, N., and Saumur, B.M., The mineral system approach applied to magmatic Ni−Cu−PGE sulphide deposits, *Ore Geol. Rev.,* 2016, vol. 76, pp. 296−316.

Barnes, J.S. and Mungall, J.E., Le Vaillant, M., et al., Sulfide−silicate textures in magmatic Ni−Cu−PGE sulfide ore deposits: disseminated and net-textured ores, *Am. Mineral.,* 2017, vol. 102, pp. 473−506.

Campbell, I.H. and Naldrett, A.J., The influence of silicate:sulfide ratios on the geochemistry of magmatic sulfides, *Econ. Geol.,* 1979, vol. 74, no. 6, pp. 1503−1506.

Cawthorn, R.G., Contrasting sulphide contents of the Bushveld and Sudbury igneous complexes, *Miner. Deposita,* 2005, vol. 40, pp. 1−12.

Chung, H.-Y. and Mungall, J.E., Physical constraints on the migration of immiscible fluids through partially molten silicates, with special reference to magmatic sulfide ores, *Earth Planet. Sci. Lett.,* 2009, vol. 286, pp. 14−22.

Feldkamp, L.A. and Jesion, G., 3-D X-ray computed tomography, *Rev Prog. Quant. NDE,* 1986, vol. 5A, pp. 555−566.

Fortin, M.−A., Riddle, J., Desjardins−Langlais, Y., and Baker, D.R., The effect of water on the sulfur concentration at sulfide saturation (SCSS) in natural melts, *Geochim. Cosmochim. Acta,* 2015, vol. 160, pp. 100−116.

Godel, B., Barnes, S.−J., and Maier, W.D., 3-D distribution of sulfide minerals in the Merensky Reef (Bushveld Complex, South Africa) and the J-M Reef (Stillwater Complex, USA) and their relationship to microstructures using X-ray computed tomography, *J. Petrol.,* 2006, vol. 47, pp. 1853−1872.

Halmshaw, R., *Non-Destructive Testing,* London: Edward Arnold, 2nd edition, 1991.

Holwell, D.A. and McDonald, I., A review of the behavior of platinum group elements within natural magmatic sulfide ore systems. The importance of semimetals in governing partitioning behavior, *Platinum Metals Reviews,* 2010, vol. 54, no. 1, pp. 26−36.

Holwell, D.A. and Keays, R.R., The formation of low-volume, high-tenor magmatic PGE−Au sulfide mineralization in closed systems: evidence from precious and base metal geochemistry of the Platinova Reef, Skaergaard intrusion, East Greenland, *Econ. Geol.,* 2014, vol. 109, pp. 387−406.

Karykowski, B.T., Maier, W.D., Groshev, N.Y., et al., Critical controls on the formation of contact−style PGE−Ni−Cu mineralization: evidence from the Paleoproterozoic

Monchegorsk Complex, Kola Region, Russia, *Econ. Geol.,* 2018, vol. 113, pp. 911−935.

Keays, R., Lightfoot, P., and Hamlyn, P., Sulfide saturation history of the Stillwater Complex, Montana: chemostratigraphic variation in platinum group elements, *Miner. Deposita,* 2011, vol. 47, pp. 151−173.

Kiseeva, E.S. and Wood, B.J., A simple model for chalcophile element partitioning between sulphide and silicate liquids with geochemical applications, *Earth Planet. Sci. Lett.,* 2013, vol. 383, pp. 68−81.

Kiseeva, E.S. and Wood, B.J., The effects of composition and temperature on chalcophile and lithophile element partitioning into magmatic sulphides, *Earth Planet. Sci. Lett.,* 2015, vol. 424, pp. 280−294.

Kislov, E.V., *Ioko−Dovyrenskii rassloennyi massiv* (Ioko−Dovyren Layered Massif), Ulan−Ude: Izd−vo Buryatskogo nauchnogo tsentra, 1998.

Konnikov, E.G., *Differentsirovannye giperbazit−bazitovye kompleksy dokembriya Zabaikal'ya* (Precambrian Differentiated Ultrabasic−Basic Complexes of Transbaikalia), Novosibirsk: Nauka, 1986.

Krivolutskaya, N. A. *Siberian Traps and Pt−Cu−Ni Deposits in the Noril'sk Area,* New York−Dordrecht−London: Psringer Chan Heidelberg, 2016.

Li, C. and Ripley, E.M., Sulfur contents at sulfide−liquid or anhydrite saturation in silicate melts: empirical equations and example applications, *Econ. Geol.,* 2009, vol. 104, pp. 405−412.

Likhachev, A.P., *Platino-medno-nikelevye i platinovye mestorozhdeniya* (PGE−Copper−Nickel and PGE Deposits), Moscow: Eslan, 2006.

Maier, W.D., Platinum−group element (PGE) deposits and occurrences: mineralization styles, genetic concepts, and exploration criteria, *J. Afr. Earth Sci.,* 2005, vol. 41, pp. 165−191.

McCuaig, T.C., Beresford, S., and Hronsky, J., Translating the mineral systems approach into an effective exploration targeting system, *Ore Geol. Rev.,* 2010, vol. 38, pp. 128−138.

Mungall, J.E., Late−stage sulfide liquid mobility in the main mass of the Sudbury igneous complex: examples from the Cictor Deep, McCreedy East, and Trillabelle deposits, *Econ. Geol.,* 2002, vol. 97, pp. 1563−1576.

Mungall, J.E. and Su Shanguo, Interfacial tension between magmatic sulfide and silicate liquids: constraints on kinetics of sulfide liquation and sulfide migration through silicate rocks, *Earth Planet. Sci. Lett.,* 2005, vol. 234, pp. 135−149.

Naldrett, A.J., *Magmatic Sulfide Deposits: Geology, Geochemistry, and Exploration,* Heidelberg−Berlin: Springer−Verlag, 2004.

Naldrett, A.J., *Fundamentals of magmatic sulfide deposits, Magmatic Ni−Cu and PGE Deposits: Geology, Geochemistry and Genesis, Rev. Econ. Geol.,* C. Li and E.M. Ripley, Eds.,

Denver: Society of Economic Geologists, 2011, vol. 17, pp. 1−50.

Orsoev, D.A., Mekhonoshin, A.S., Kanakin S.V., et al., Gabbro−peridotite sills of the Late Riphean Dovyren plutonic complex (northern Baikal area, Russia), *Russ. Geol. Geophys.,* 2018, vol. 59, no. 5, pp. 472−485.

Pearce, M.A., Godel, B.M., Fisher, L.A., et al., Microscale data to macroscale processes: a review of microcharacterization applied to mineral systems, *Characterization of Ore-Forming Systems from Geological, Geochemical and Geophysical Studies,* Gessner, K., Blenkinsop, T.G., and Sorjonen-Ward, P., Eds., *Geol. Soc. London: Spec. Publ.,* 2017, vol. 453.
https://doi.org/10.1144/SP453.3

Ripley, E.M. and Li, C., Sulfide saturation in mafic magmas: is external sulfur required for magmatic Ni−Cu−(PGE) ore genesis?, *Econ. Geol.,* 2013, vol. 108, pp. 45−58.

Robertson, J.C., Barnes, J.S., and Le Vaillant, M., Dynamics of magmatic sulphide droplets during transport in silicate melts and implications for magmatic sulphide ore formation, *J. Petrol.,* 2016, vol. 56, pp. 2445−2472.

Rontgen, W., Uber eine neue art von strahlen (concerning a new type of radiation), *Annu. Rev. Phys. Chem., New Ser.,* 1989, vol. 64, pp. 1−37.

Sinyakova, E.F. and Kosyakov, V.I., Physicochemical prerequisites for the formation of primary orebody zoning at copper−nickel sulfide deposits (by the example of the systems Fe−Ni−S and Cu−Fe−S), *Russ. Geol. Geophys.,* 2012, vol. 53, no. 9, pp. 1126−1153.

Sinyakova, E.F., Kosyakov, V.I., and Borisenko, A.S., Effect of the presence of As, Bi, and Te on the behavior of Pt metals during fractionation crystallization of sulfide magma, *Dokl. Earth Sci.,* 2017, vol. 477, no. 4, pp. 1422−1426.

Smol'kin, V.F., Fedotov, Zh.A., Neradovskii, Yu.N., et al., *Rassloennye intruzii Monchegorskogo rudnogo raiona: petrologiya, orudenenie, izotopiya, glubinnoe stroenie* (Layered Intrusions of the Monchegorsk Ore District: Petrology, Mineralization, Isotopy, and Deep Structure), Apatity: Kol'sk. Nauchn. Ts. RAN, 2004.

Spiridonov, E.M., Ore-magmatic systems of the Noril'sk ore field, *Russ. Geol. Geophys.,* 2010, vol. 51, pp. 1059−1077.

Tolstykh, N.D., Orsoev, D.A., Krivenko, A.P., and Izokh, A.E., *Blagorodnometall'naya mineralizatsiya v rassloennykh ul'trabazit−bazitovykh massivakh yuga Sibirskoi platformy* (Noble Metal Mineralization in the Layered Ultrabasic−Basic Massifs of the Southern Siberian Platform), Novosibirsk: Parallel', 2008.

Translated by E. Kurdyukov